Journal of the Mechanical Behavior of Biomedical Materials 180 (2026) 107476

Contents lists available at ScienceDirect

Journal of the Mechanical Behavior of Biomedical Materials

journal homepage: www.elsevier.com/locate/jmbbm

Research paper

From human joints to bioreactor setups: Quantifying mechanical stimuli in cartilage physiology and regeneration

Satanik Mukherjee [a,b,*], Wouter Wilson [c], Liesbet Geris [a,b,d]

[a] Biomechanics Section, KU Leuven, Leuven, Belgium
[b] Prometheus, Division of Skeletal Tissue Engineering, KU Leuven, Leuven, Belgium
[c] TU Eindhoven, Eindhoven, Netherlands
[d] GIGA Institute, University of Liege, Liege, Belgium

ARTICLE INFO

Keywords:
Bioreactors
Knee joint mechanics
Osteochondral explants
Cartilage tissue engineering
Finite element analyis

ABSTRACT

Bioreactors are widely used to apply mechanical stimuli to osteochondral (OC) explants and cartilage tissue-engineered (TE) constructs, yet their ability to replicate native joint mechanics is not well quantified. Using a finite element (FE) modeling approach, this study benchmarks common bioreactor loading protocols against the human knee during gait, enabling direct comparison to physiologically relevant mechanical parameters.

A validated FE model of the human knee joint simulating the stance phase of gait was used to characterize key mechanical variables: maximum principal stress, maximum shear strain, pore pressure, and fluid velocity. These outputs were compared with FE analyses of representative bioreactor setups: dynamic unconfined compression (UC) (10%–30%) and combined compression (10%) with ball rotation (±25°), applied to both OC plugs and TE constructs, and hydrostatic pressure (0.5–50 MPa), applied only to TE constructs.

In OC plugs, 10% UC generated maximum principal stresses (~7.5 MPa) and pore pressures (~4 MPa) closely matching native tissue (~4.5 MPa and ~5 MPa, respectively). In TE constructs, even at 30% UC, maximum principal stresses and pore pressures remained around 100 times lower than physiological values, while fluid velocities were 10 times higher. Hydrostatic loading of TE constructs at 5 MPa matched native pore pressures (~5 MPa) but induced negligible strains.

This study establishes a quantitative framework for evaluating how well bioreactor loading regimens replicate physiological joint mechanics. While limited to a single-subject dataset, this framework provides a robust *in silico* benchmarking methodology and identifies comparative indicators for evaluating bioreactor setups against specific mechanical variables. This work lays the foundation for a more standardized design of *in vitro* cartilage studies, supporting targeted translational strategies in cartilage repair and tissue engineering.

1. Introduction

Mechanical loading plays a crucial role in maintaining articular cartilage homeostasis. Non-physiological mechanical loading, including both hypo-physiological loading, as seen during joint immobilization, and hyper-physiological loading, as encountered during traumatic joint injuries, are linked to degenerative changes in cartilage (Griffin and Guilak, 2005; Bader et al., 2011; Gilbert and Blain, 2018). Articular cartilage is a biphasic tissue, consisting of a solid phase mainly composed of proteoglycans and collagen fibrils, and a fluid phase. In healthy cartilage, the majority of load-bearing is achieved through pore fluid pressurization. Additionally, there is an arcade-like pattern of collagen fibril orientation across the thickness of cartilage, especially in weight-bearing joints such as the hip and knee. This unique arrangement gives cartilage an anisotropic behavior, allowing it to resist shear forces along the surface. During daily activities, articular cartilage is subjected to a wide range of mechanical stimuli, creating a complex dynamic state of stresses and strains at various anatomical locations within the joint.

In cartilage tissue engineering (TE), bioreactors are used to culture tissue engineered constructs under controlled mechanical conditions. Bioreactors furthermore provide an *ex vivo* platform for studying the effects of mechanical loading on disease progression, such as osteoarthritis (OA) and possible therapeutic interventions. In literature, bioreactors used in context of cartilage (patho)physiology and regeneration can be broadly classified into dynamic compression, combined dynamic compression and shear, and hydrostatic pressure (Natenstedt et al., 2015; Salinas et al., 2018). Dynamic compression bioreactors

* Corresponding author.
E-mail address: satanik.mukherjee@kuleuven.be (S. Mukherjee).

https://doi.org/10.1016/j.jmbbm.2026.107476
Received 27 December 2025; Received in revised form 23 May 2026; Accepted 24 May 2026
Available online 1 June 2026

are designed to replicate the compressive strains experienced by knee cartilage. Bioreactors that combine compression and shear aim to reproduce the complex multiaxial loading environment present in the joint. Hydrostatic pressure bioreactors are intended to emulate the pore fluid pressurization within articular cartilage, which plays a key role in load bearing. Despite the widespread use of these bioreactors in the literature, there is considerable variability in the corresponding mechanical loading protocols applied in these bioreactors, which can lead to inconsistencies in the outcomes of different studies (Salinas et al., 2018). While multiple review articles exist that compare these different bioreactors (and loading conditions) to their respective outcomes in terms of cellular response (Natenstedt et al., 2015; Salinas et al., 2018), no such broad efforts have been made to compare quantitatively what are the differences in mechanics encountered in these different setups and how closely they replicate the *in vivo* physiological scenario.

Capturing the detailed mechanics of TE constructs or explants subjected to mechanical loading in bioreactors is very difficult using traditional experimental techniques due to the complexity of mechanical environment that exists within the specimens. In this context, *in silico* models have been established as an enabling technology to quantify the mechanical environment in these setups as well as human joints (Geris et al., 2018; Mukherjee et al., 2020). In particular finite element (FE) analysis has been widely used in literature to quantify the mechanics of constructs or explants in many bioreactor studies (Babalola and Bonassar, 2009; Zahedmanesh et al., 2014; Bandeiras et al., 2014; Hassan et al., 2019; Elahi et al., 2021, 2023). However, most of these studies focus on a single type of bioreactor only, thereby making it difficult to make a comparative analysis across different types of bioreactors and corresponding loading protocols. Furthermore, these studies do not incorporate a model of the *in vivo* scenario which the bioreactor aims to recapitulate as a quantitative basis of comparison.

The present study aims to bridge this gap in literature by performing a comparative analysis of widely used bioreactor setups in the literature with a physiological human knee joint model, utilizing FE analysis. This study will not only provide a better understanding of the differences in mechanical environment across different bioreactor setups, but will also provide an extensive repository of bioreactor setups and loading conditions for experimentalists to choose from, depending on the research question to be studied. To achieve this aim, firstly, an FE model of the human knee joint is developed using geometry and material properties obtained from literature. Secondly, FE models of bioreactors applying mechanical loading to osteochondral grafts and TE constructs are developed. Lastly, a comparative analysis is conducted between the optimal loading cases of each bioreactor type and the human knee joint. This analysis will help identify the loading regimes specific to each bioreactor setup that most closely mimics specific mechanical aspects of the physiological situation.

2. Methods

2.1. FE modeling of the human knee joint

The tibiofemoral joint geometry of a cadaveric right knee (70-year-old female, 77.1 kg, 1.68 m) was obtained from the Open Knee database (Erdemir, 2016) and imported into Abaqus 2023 (SIMULIA, Providence, RI, USA) for FE analysis. Model development details are provided in Supplementary Data S1. Briefly, articular cartilage was modeled as a biphasic, fibril-reinforced poroviscoelastic (FRPVE) material, as described previously (Wilson et al., 2004; Quiroga et al., 2017). The solid matrix was composed of two main components: collagen fibrils (fibrillar) and proteoglycans (non-fibrillar). A depth-dependent, arcade-like orientation was applied to the primary collagen fibrils to represent their natural organization through the cartilage thickness. Additionally, split-line patterns were incorporated on the cartilage surface to reflect the preferred in-plane orientation of the collagen network (Fig. 1(c)). Material parameters for all tissues are listed in Supplementary Table S1.

Boundary conditions simulating the stance phase of gait, including time-dependent axial force, anterior–posterior translation, and internal–external and flexion-extension rotations were applied to the femur, based on Mononen et al. (2015). The joint axial force was obtained from the data set of Mononen et al. (2015), which was for a person weighing 100 kg. It was scaled by 0.77 to match the weight (77 kg) of the person for which the FE analysis was performed in this study (Erdemir, 2016). Boundary conditions were applied at a reference point centered between the femoral epicondyles (Fig. 1(b)). The tibia was fully constrained.

2.2. FE modeling of bioreactors for osteochondral plugs

Three-dimensional FE models of the osteochondral plugs were created in Abaqus, with an 8 mm diameter based on literature (Schwab et al., 2021; Kleuskens et al., 2021). Model development details are provided in Supplementary Data S2. Briefly, the osteochondral plugs consisted of cartilage (2 mm thick considering average human cartilage thickness), calcified cartilage (0.2 mm thick Evans and Pitsillides, 2022) and 4 mm of subchondral bone underneath. The subchondral bone was further subdivided into subchondral cortical bone (0.36 mm thick) and subchondral trabecular bone (3.64 mm thick) (Rapagna et al., 2021). The corresponding tissues were rigidly attached to one another using a 'Tie constraint'. Cartilage was modeled as a fibril-reinforced poroviscoelastic material as described in section 2.1. Calcified cartilage, subchondral cortical and trabecular bone were modeled as linear elastic materials with material parameters obtained from literature (Stender et al., 2017), and mentioned in Supplementary Table S1.

The osteochondral plugs were subject to mechanical loading in two different bioreactor setups that are commonly used in literature to apply unconfined compression, and combined compression and shear, respectively. The boundary conditions that were applied to mimic mechanical loading in FE model of the bioreactors are described below (Fig. 2).

(a) Dynamic unconfined uniaxial compression bioreactor: this bioreactor is most commonly used in literature for its simplicity in design and ease of application of mechanical loading (Sah et al., 1989; Li et al., 2013). Uniaxial dynamic compression was applied to the plugs in the FE model by using a rigid impermeable plate with a diameter of 12 mm. A haversine function with a frequency of 1 Hz and amplitudes of 10%, 20%, and 30% of the initial cartilage thickness was defined at the reference point of the rigid plate to impart dynamic compression to the plugs. The loading amplitudes were selected to encompass the wide range of mechanical loading regimes mentioned in literature (Li et al., 2013; Patel et al., 2019).

To assess the role of individual tissues in the stress response of osteochondral plugs subject to uniaxial compression, three cases were simulated by progressively excluding specific tissues (Fig. 2):

- All: included cartilage, calcified cartilage and subchondral bone
- No calcified cartilage (NoCC): calcified cartilage was excluded
- Only cartilage: 2 mm thick cartilage layer only

(b) Dynamic multi-axial loading bioreactor: to replicate physiological multi-axial loading, bioreactors combining axial compression and shear have been developed in literature, notably using a 32 mm ceramic hip ball as described in studies from AO Davos, Switzerland (Wimmer et al., 2004; Grad et al., 2012; Vainieri et al., 2018). In this configuration, axial load is applied via vertical displacement of the ball, while shear is generated by rotating the ball about an axis perpendicular to the loading direction. An FE model of this setup was developed in this study, with the ceramic ball modeled as a rigid body. A friction coefficient of 0.02 (Guilak, 2005) was applied between the cartilage and ceramic ball using the 'Lagrange Multiplier' friction

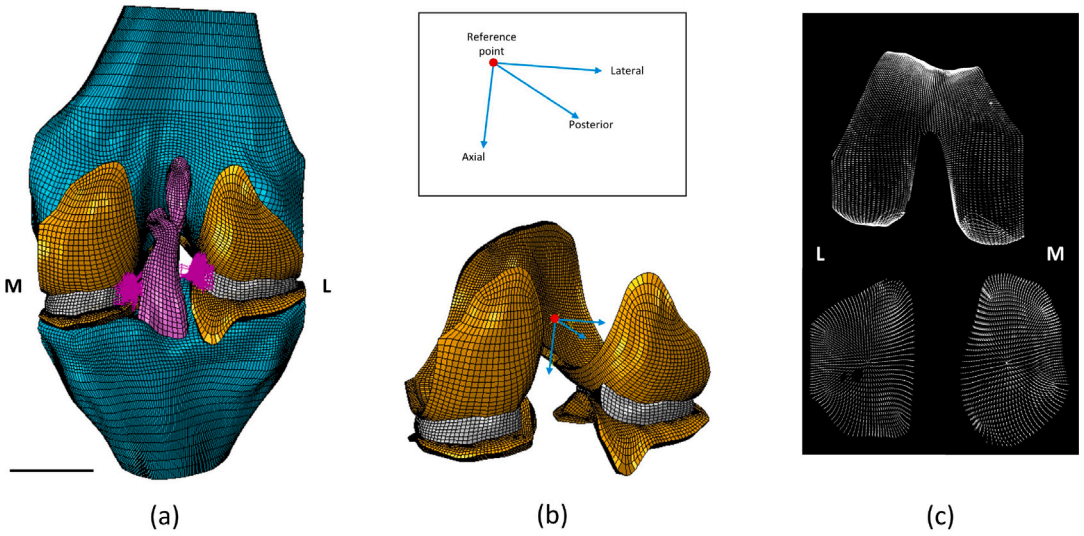

Fig. 1. (a) FE model of the human knee joint with the different tissues and meniscal attachment springs (in pink), M-medial, L-lateral, Scale bar = 20 mm; (b) The reference point and the axes about which boundary conditions are applied for the FE model (ligaments and bones have been removed for visualization). In the inset box, a zoomed in view showing the reference point and axes with anatomical directions; (c) Orientation of the split-line patterns at the superficial zone as implemented in the FE model.

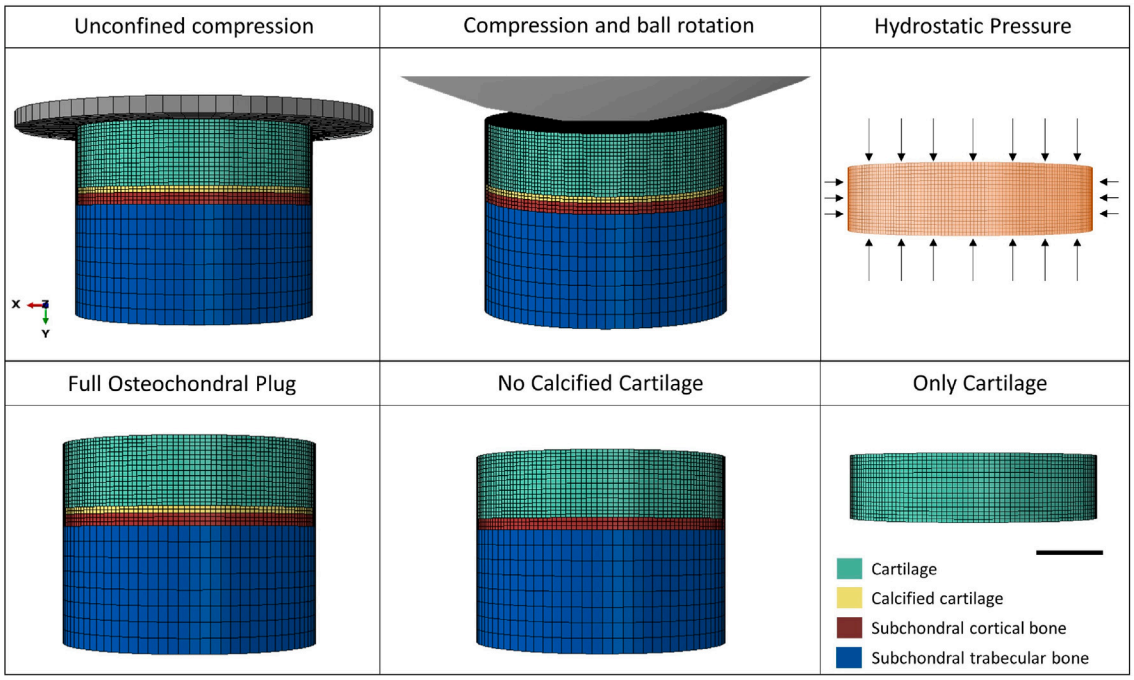

Fig. 2. Top row: Different types of bioreactors used in the study. The first two from left show osteochondral plugs, while hydrostatic pressure was applied to only TE constructs. A portion of the ball is visualized in the compression and ball rotation case. Bottom row: FE models to study the role of different tissues in osteochondral plugs. Scale bar = 2 mm.

formulation. Boundary conditions were applied to a reference point at the center of the ball, with four loading conditions tested in this setup:

(1) 10% quasi-static compression for 10 s,

(2) 10% quasi-static compression, followed by 10% dynamic loading at 1 Hz,

(3) 10% quasi-static compression, followed by ±25 degrees dynamic rotation at 1 Hz,

(4) 10% quasi-static compression, followed by 10% dynamic loading and ±25 degrees dynamic rotation at 1 Hz.

All dynamic conditions were simulated for five cycles in the FE model. Results were analyzed at the peak of the fifth cycle to ensure that the initial transient effects had dissipated.

2.3. FE modeling of bioreactors for cartilage tissue engineered constructs

The TE constructs were modeled as 8 mm diameter, 2 mm thick discs. The dimensions were kept consistent with those of the cartilage in osteochondral plugs to ensure dimensional conformity when comparing the simulation outcomes. Agarose, a commonly used hydrogel in cartilage TE, was selected as the construct material. Its non-linear, compressible poroelastic behavior was modeled using a hyperfoam formulation with strain-dependent permeability, as in previous studies (Buschmann et al., 1992; Khoshgoftar et al., 2011). Further details of the FE model development are provided in Supplementary Data S3.

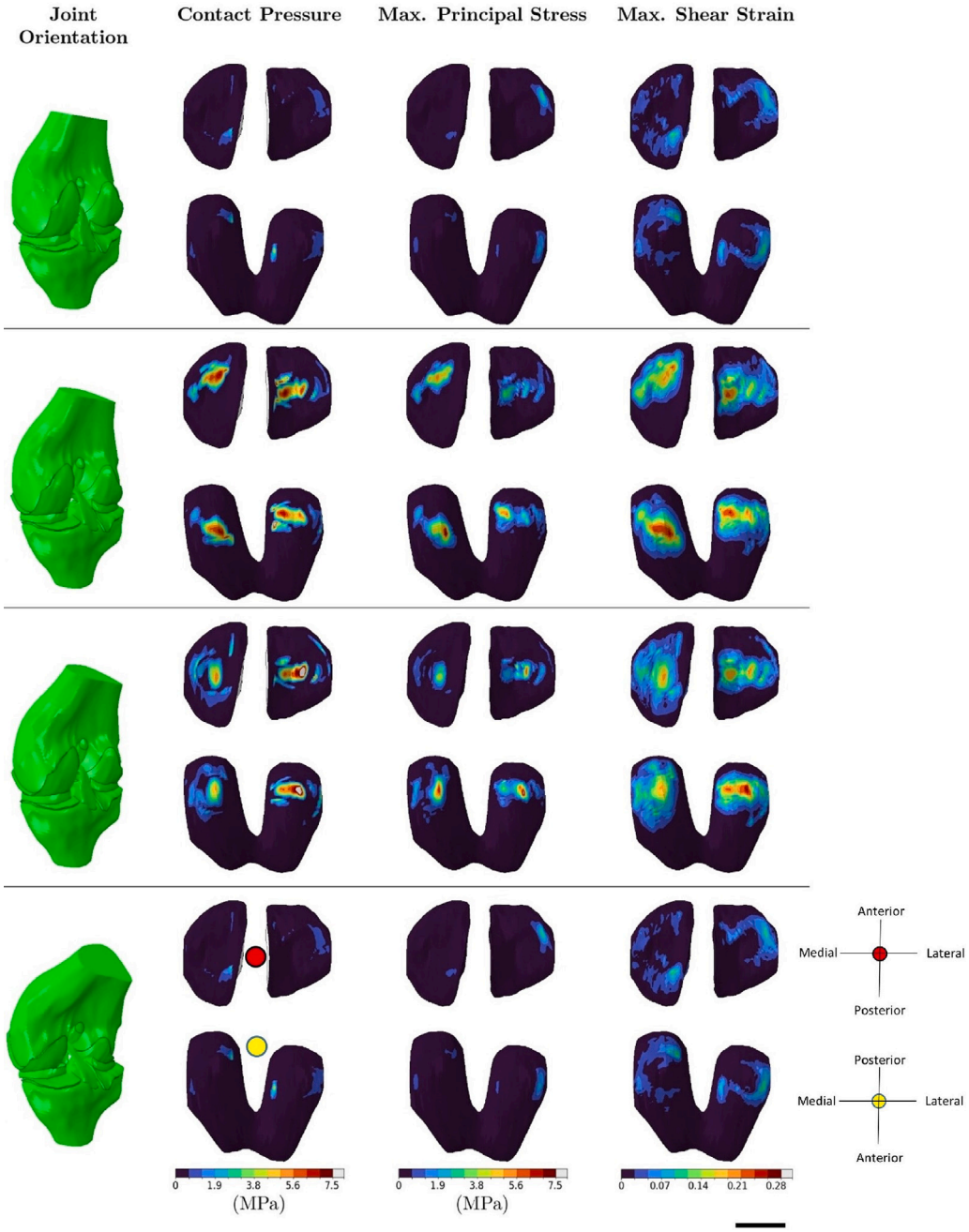

Fig. 3. FE analysis of human knee joint during stance phase of gait showing results at fraction of stance 0, 0.2, 0.82, 1 starting from the top. Joint orientation is shown at the corresponding stance fraction. Red and yellow dots are used as indicators to show the relevant anatomical direction in context of the figures, where the tibial and femoral cartilage are displayed. Scale bar = 20 mm.

The TE constructs were subjected to mechanical loading using three bioreactor setups simulating unconfined compression, combined compression-shear, and hydrostatic pressure. Boundary conditions for the first two cases were same as that for osteochondral plugs (explained in Section 2.2(a), (b)), except a friction coefficient of 0.1 was used between the TE construct and loading surfaces (Geurds et al., 2021).

Dynamic hydrostatic pressure bioreactor: for knee articular cartilage *in vivo*, most of the compressive forces are transferred to hydrostatic pressure (HP) due to interstitial fluid pressurization, which acts as a primary load bearing mechanism in joints (Hodder et al., 2020). To harness this hydrostatic pressure to stimulate cartilage production in TE constructs, hydrostatic bioreactors have been used to impart a wide range of pressure magnitudes and frequencies (Elder and Athanasiou, 2009; Hodder et al., 2020; Chariyev-Prinz et al., 2023). In the present study, FE analysis of TE constructs subjected to static (0 Hz) and dynamic hydrostatic pressure (at a frequency of 1 Hz) were performed. The magnitudes for hydrostatic pressure application were 0.5 MPa, 5 MPa, 10 MPa and 50 MPa, which were chosen to cover the wide range of magnitudes reported in literature (Hodder et al., 2020). The hydrostatic pressure was applied using a 'Pressure Load' in Abaqus.

3. Results

3.1. FE analysis of the human knee joint

The results of FE simulations of stance phase of gait in the human knee joint revealed that at the first peak loading (at 20% of the stance phase of gait), contact pressures were balanced between the

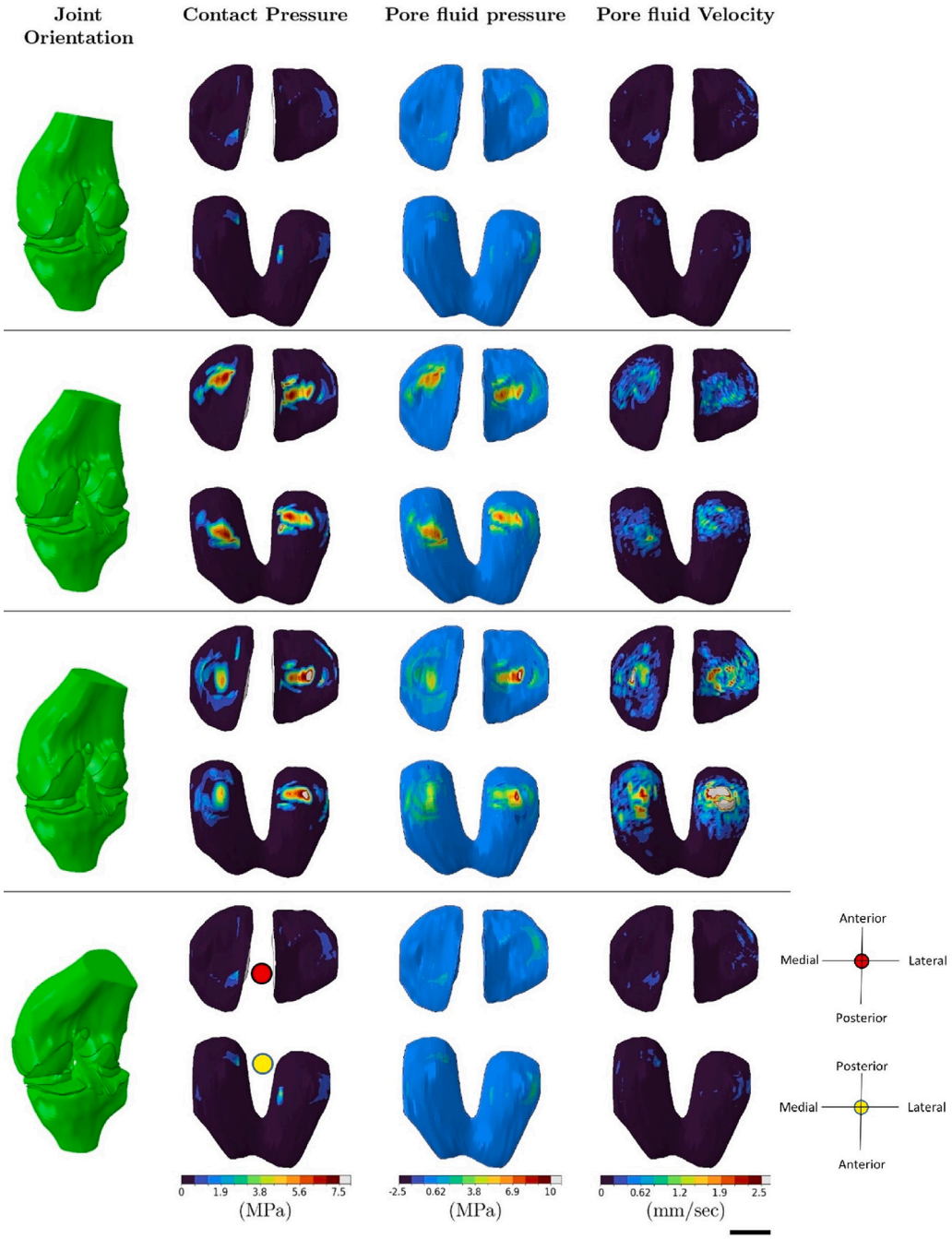

Fig. 4. FE analysis of human knee joint during stance phase of gait showing results at fraction of stance 0, 0.2, 0.82, 1 starting from the top. Joint orientation is shown at the corresponding stance fraction. Red and yellow dots are used as indicators to show the relevant anatomical direction in context of the figures, where the tibial and femoral cartilage are displayed. Scale bar = 20 mm.

medial and lateral compartments of the joint as observed in Fig. 3. During the second peak loading (at 81.7% of the stance phase of gait), the contact pressures were higher on the lateral compartment of the tibial and femoral cartilage, suggesting a shift in load bearing towards the lateral compartment during the second peak loading of the gait cycle. This observation goes in line with previous observations in literature (Mononen et al., 2015), where a gradual shift in load from the medial to the lateral compartment was observed as well. Similar trends were observed for maximum principal stress, pore pressure, pore fluid velocity and maximum shear strain as seen in Figs. 3, 4. At the contact region between the femoral and tibial cartilage (Fig. 8), the highest maximum principal stresses were observed in the superficial zone (SZ) and middle zone (MZ), while maximum shear strain peaked at the cartilage surface at the point of contact. The varus–valgus rotations obtained from the simulations were within the range that was observed in experimental studies (Figure S13; S: Supplementary Material).

3.2. Role of calcified cartilage and subchondral bone in unconfined compression of osteochondral grafts

The removal of calcified cartilage from the osteochondral plug (noCC case) in simulations led to higher maximum principal stresses being transferred from the cartilage to the subchondral cortical bone for all three magnitudes of uniaxial compression (ranging from 10% to 30% strains) as compared to the intact osteochondral plug (all tissues present) (Fig. 5). Additionally, there was an increase in the pore fluid

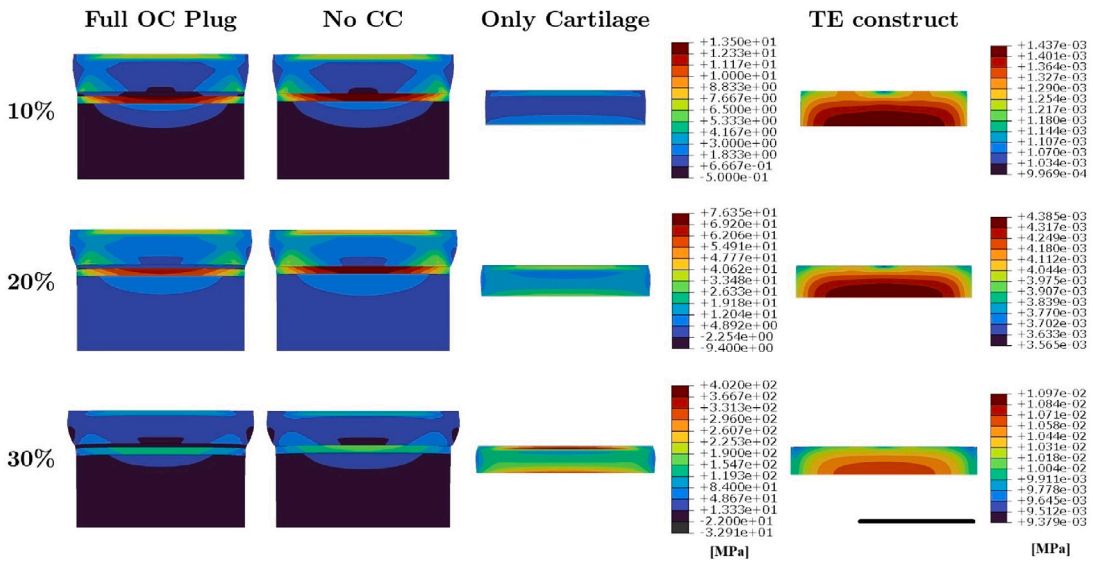

Fig. 5. Distribution of maximum principal stress (in MPa) in different tissues of the OC plug and the TE construct for 10%, 20% and 30% strain applied in dynamic unconfined compression with 1 Hz frequency. NoCC - No Calcified Cartilage. Scale bar = 5 mm.

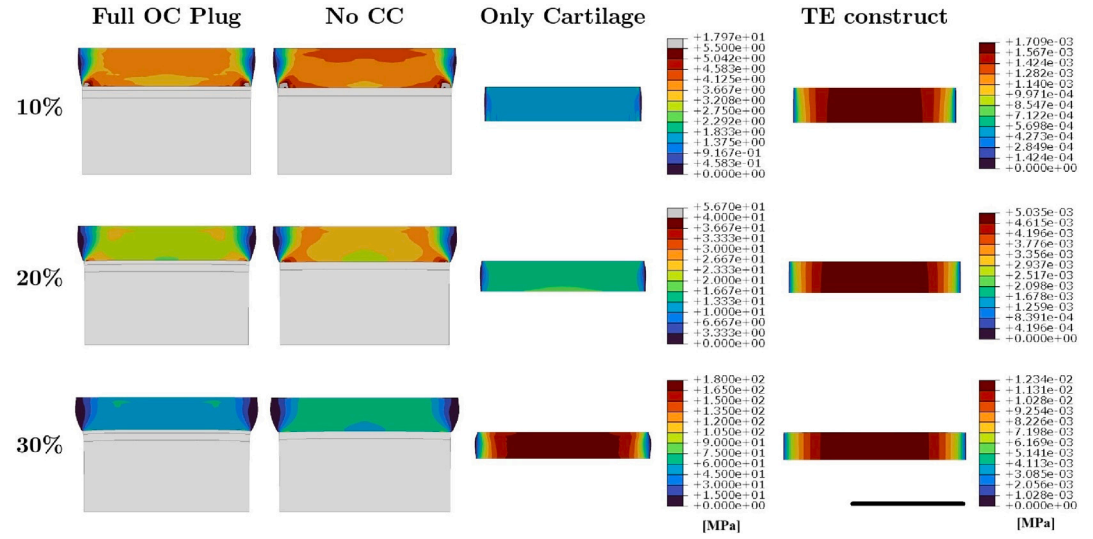

Fig. 6. Distribution of pore fluid pressure (in MPa) in different tissues of the osteochondral (OC) plug and the tissue engineered (TE) construct for 10%, 20% and 30% strain applied in dynamic unconfined compression with 1 Hz frequency. NoCC - No Calcified Cartilage. Scale bar = 5 mm.

pressure and fluid velocity around the cartilage circumference near the junction due to the absence of calcified cartilage (Figs. 6, S8). For compression of only cartilage plugs, the lack of bone–cartilage interface resulted in a more uniform distribution of shear strains compared to the previous two cases (Figure S7). In the cartilage-only case, a spike in pore fluid velocity was observed at the top circumference of the cartilage, whereas, in the other two cases, the spike occurred in the cartilage circumference at the cartilage–bone interface (Figure S8). Overall values of pore pressure in cartilage were consistently higher (by approx 30%) for the no CC case as compared to the full OC plugs consistently across the 3 loading regimes (Fig. 6).

3.3. Mechanical influence of combined dynamic compression and sliding rotation of ceramic ball

Dynamic compression with the ceramic ball resulted in higher maximum principal stresses at the center of the contact area in both OC plugs and TE constructs (Figure S9). In cartilage, highest stresses were observed at the SZ-MZ interface. Pore pressure was highest beneath the contact center (Figure S11), while fluid velocity peaked at the contact edge between the ball and the cartilage (or TE construct) (Fig. 7).

Rotational motion of the ceramic ball had negligible mechanical effects on cartilage. However, rotation of the ball caused asymmetric distributions of maximum principal stress, maximum shear strain, pore pressure, and fluid velocity in TE constructs, especially causing higher magnitudes in the leading direction of rotation (Figs. 7, S9, S10, S11). This asymmetry during rotation of the ball was due to the higher friction coefficient between the ceramic ball and agarose TE construct.

3.4. Comparative analysis of the most-physiological cases from each bioreactor type

Mechanical loading conditions from each bioreactor that most closely replicate *in vivo* knee joint cartilage mechanics during the first peak of the stance phase were selected for comparison (Fig. 8). The analysis focused on four key mechanical variables: maximum principal stress, maximum shear strain, pore fluid pressure and fluid velocity. Maximum principal stress was chosen for its role in collagen fiber

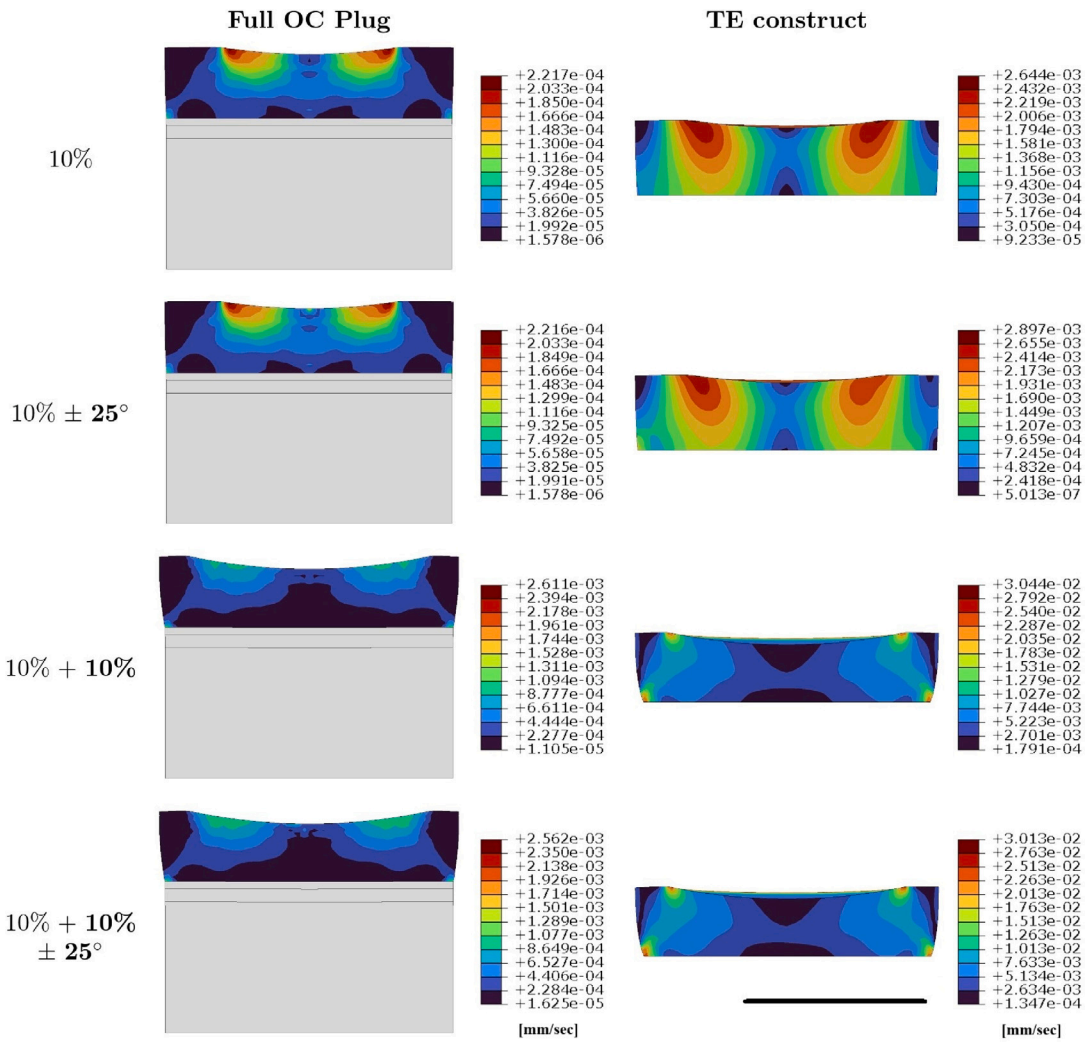

Fig. 7. Distribution of pore fluid velocity (in mm/sec) in OC plug and the TE construct for 4 different conditions of applied compression with ball rotation. Values in bold in the first column represents a dynamic boundary condition with 1 Hz frequency, while normal fonts are for quasi-static. Scale bar = 5 mm.

damage (Mononen et al., 2016), pore pressure for its relevance in cartilage load bearing (Hodder et al., 2020), and fluid velocity for its role in loss of fixed charge density in cartilage, especially at cartilage lesions (Orozco et al., 2018). Maximum shear strain was chosen for its role in proteoglycan loss (Eskelinen et al., 2019) as well as cell apoptosis and cell death (Bonnevie et al., 2018; Kosonen et al., 2023), particularly during injurious loading of cartilage. Medial tibial and femoral cartilage were used for comparison, as this compartment experiences the highest magnitudes of these variables during the first peak loading phase.

10% Dynamic unconfined compression of OC plugs: in this case, the cartilage of OC plug exhibited maximum principal stress magnitudes and distributions similar to those in medial knee cartilage, with peak stresses concentrated in the SZ at the interface with the MZ. This aligns with previous studies reporting high strain concentrations and subsurface cartilage delamination at the SZ-MZ interface due to repetitive compressive loading (Neu et al., 2005; Durney et al., 2020; Petersen et al., 2023). Additionally, stress patterns near the cartilage-calcified cartilage interface were comparable. In both the OC plug and native cartilage, a central low-stress region beneath the contact area was flanked by zones of high stress at the bone–cartilage (or calcified cartilage) interface (Fig. 8).

Maximum shear strain also followed a similar gradient in both models, decreasing from the surface to the deeper zones. Unlike principal stress, maximum shear strain was not concentrated in the SZ but was more evenly distributed. While principal stress is influenced by tension in surface-aligned collagen fibers, shear strain depends on the shear modulus of proteoglycan-rich matrix components. This difference in mechanisms of load bearing of the cartilage constituents might explain the difference in distribution of the stress components.

Pore pressure distributions were also similar, approaching zero near the free-draining surfaces in both the knee and OC plug. However, pore pressure magnitude was lower in the OC plug. Pore fluid velocity was highest near the contact area in knee cartilage. In the OC plug, peak fluid velocities occurred along the curved free-draining surface, where a zero pore pressure boundary condition was applied.

30% Dynamic unconfined compression of TE constructs: due to the low stiffness of agarose, stresses in the TE construct were 2 orders of magnitude lower than in knee cartilage, even under 30% compression. Maximum principal stress and shear strain were uniformly distributed across the construct thickness, unlike knee cartilage where SZ stresses are higher due to collagen fiber alignment. Maximum shear strain was twice that of knee medial cartilages. Fluid velocity was 10 times higher and pore pressure 100 times lower than in knee cartilage. However, the spatial distributions were qualitatively similar, with elevated pore pressures in the central region of both the construct and cartilage contact area, and increased fluid velocities near the edges of the construct and at the periphery of the cartilage contact region, respectively.

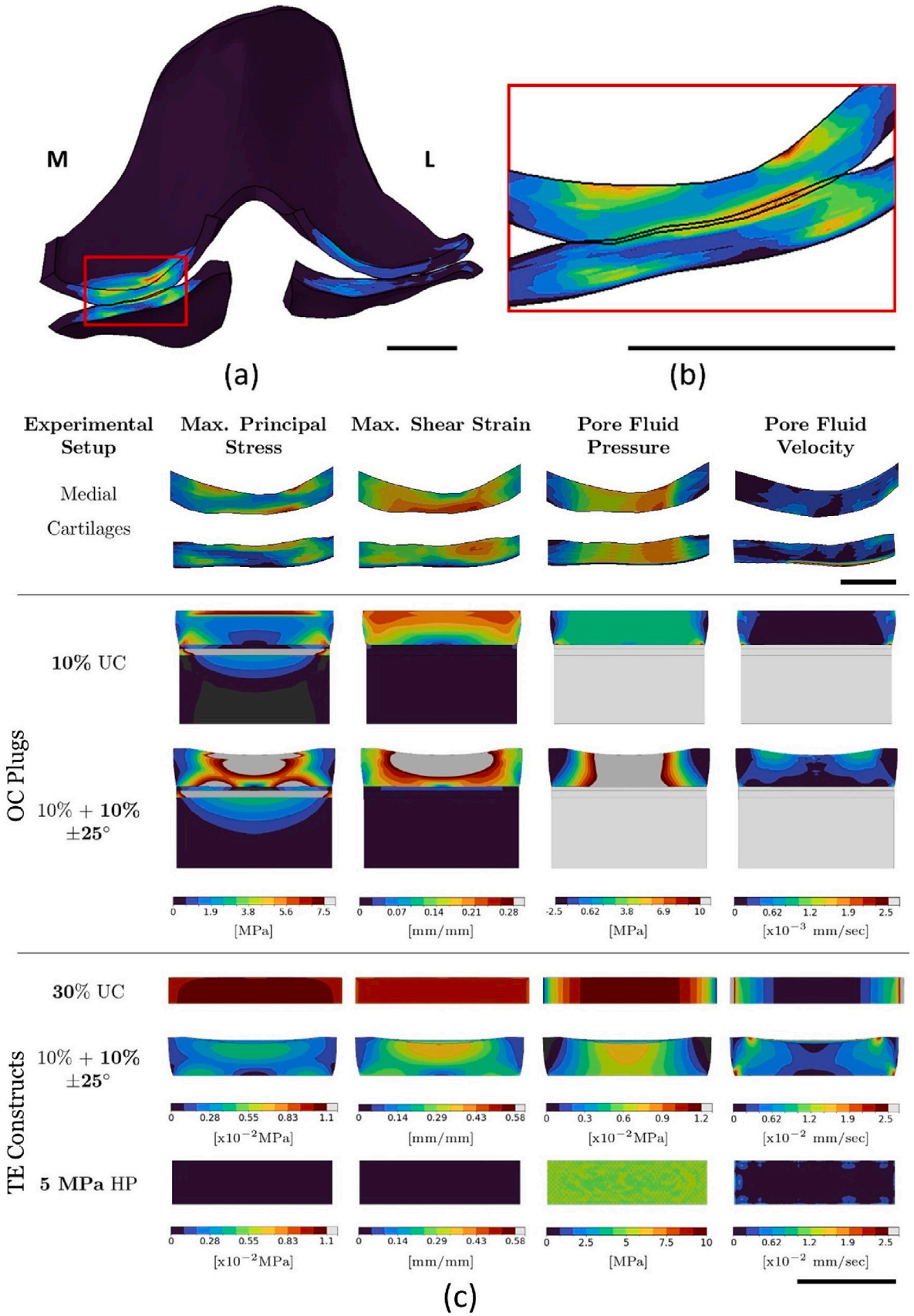

Fig. 8. (a) Cut section of the knee joint at the first peak loading, the red box shows region of medial cartilage under contact, for which results were analyzed, Scale bar = 10 mm; (b) Zoomed in view of the contact region in (a), Scale bar = 10 mm; (c) Comparison of physical variables between the different conditions of mechanical loading of OC plugs and TE constructs with the medial cartilage region selected as in (a), (b). In (c), overlapping tibial and femoral cartilages were separated to facilitate visualization of the mechanical variable distributions. UC- Unconfined Compression, HP- Hydrostatic Pressure, applied at a frequency 1 Hz. Scale bar = 5 mm.

Dynamic compression and sliding motion applied to OC plugs: a quasi-static compression of 10% followed by a 10% dynamic compression and simultaneous ±25° dynamic rotation of the ball was chosen for comparison with the knee articular cartilage. The values of all the 4 mechanical variables obtained from this bioreactor condition were higher in magnitude than the ones observed for knee cartilage (Fig. 8). High maximum principal stress and pore fluid pressure distributions were observed at a region in the center of cartilage under the contact area of the ball with the cartilage, similar to the area underneath cartilage to cartilage contact in the knee joint. Highest values of maximum principal stress and maximum shear strain were located in the SZ. Pore fluid velocity in the OC plug followed similar distribution and magnitude, with highest magnitudes occurring towards the edge of the contact (between the ball and cartilage) and close to the top surface, similar to the knee cartilage.

Dynamic compression and sliding motion applied to TE constructs: for the same 10% dynamic compression and ±25° sliding motion as in the previous case, maximum shear strain close to the TE construct surface was significantly higher (around double) than that observed for knee joint cartilage. Distribution of both maximum principal stress and maximum shear strain followed a gradient across the construct thickness with higher values closer to the contacting surface, similar to what is observed in knee articular cartilage. The magnitudes of pore fluid pressure and velocity followed similar trends as observed for the unconfined compression of TE constructs as described above.

Dynamic Hydrostatic Pressure on TE Constructs: applying 5 MPa dynamic hydrostatic pressure produced a nearly uniform pore pressure in TE constructs, with magnitudes comparable to those observed in the knee cartilage beneath contact areas. This was the only setup that successfully mimicked physiological pore pressure in TE constructs despite their high permeability. However, other mechanical variables remained significantly lower than in native cartilage, highlighting the limitation of this method in replicating full mechanical behavior.

4. Discussion

The present *in silico* study compared FE models of common bioreactor setups used to apply mechanical stimuli to osteochondral explants and cartilage TE constructs against an FE model of the human knee joint simulating stance phase of gait. While prior studies have examined mechanics of individual bioreactors (Tanck et al., 1999; Bandeiras et al., 2014; Zahedmanesh et al., 2014; Hassan et al., 2019), this work uniquely benchmarks them against an *in vivo* physiological reference, enabling a more informed assessment of how closely each setup replicates native joint mechanics.

It should be noted, however, that the *in vivo* reference is derived from a single subject, which limits its generalizability across the population. Furthermore, the geometry and load datasets originate from two different individuals, which may introduce reference frame inconsistencies and could partly explain the lateral-dominant loading pattern observed in our model during the second peak loading of the gait cycle. While lateral-predominant loading is less common, the stresses and contact pressures obtained in our study fall within the range of inter-subject variability reported in the literature (Mononen et al., 2015). Given that the medial compartment statistically bears the majority of the load during gait, and that contact pressures were more evenly distributed across both compartments at first peak loading, the medial compartment at first peak load was selected as the most physiologically representative baseline for comparison with the bioreactor studies. Future work incorporating multiple subjects with matched datasets will be essential to quantify inter-subject variability and establish more robust ground truth targets for bioreactor loading protocols.

This study revealed that no single bioreactor replicated all mechanical variables in both magnitude and spatial distribution. However, the findings offer guidance for selecting bioreactors based on specific research goals. For instance, 10% unconfined compression of OC plugs matched native cartilage in terms of stress and pore fluid pressure, but fluid velocity patterns differed. In TE constructs, unconfined compression (up to 30%) produced stresses and pore fluid pressures 2–3 orders of magnitude lower than in knee cartilage. Hydrostatic pressure of 5 MPa applied to TE constructs better approximated native cartilage pore pressures, though it induced much lower strains.

The 8 mm diameter of the OC plugs was chosen to match the typical cartilage-to-cartilage contact area (6–10 mm) during peak gait loading. Unlike *in vivo* cartilage, which is laterally constrained by surrounding tissue, the OC plugs had free lateral surfaces that allowed unrestricted bulging and fluid outflow. Consequently, unconfined compression produced higher fluid velocities at the plug perimeter, creating an 'edge effect.' Such elevated fluid velocities may contribute to matrix loss at the lateral surface, as observed in some *in vitro* studies (Li et al., 2013), especially given peripheral damage of cartilage from plug harvesting.

For the combined compression and ball-rotation simulations, ball rotation had a negligible influence on cartilage mechanics, but was retained in the comparative analysis because it mimics the sliding motion during gait that stimulates lubricin production in the SZ, which helps maintain low friction (Grad et al., 2012). This apparent discrepancy between observed mechanics from FE analysis and lubricin production suggests that the biological response to sliding is driven by surface-level mechanical phenomena that operate below the resolution of the current continuum-level model. Sliding motion might generate local fluid-induced shear at the articular surface that has been shown to promote lubricin expression specifically in superficial zone chondrocytes via CREB-dependent mechanotransduction pathways (Ogawa et al., 2014). Since the current FE model does not simulate fluid film dynamics at the contact interface, these surface-level stimuli are not captured. This finding further underscores the need for future models incorporating fluid–structure interaction at the contact interface to fully explain how rotation-induced stimuli translate into biological responses such as lubricin upregulation. A related limitation of the current study is the omission of contact area migration in the bioreactors, whereby the contact area moves across the articular surface during loading. Contact migration plays an important role in maintaining fluid pressurization and reducing friction in native cartilage (Caligaris and Ateshian, 2008). This migration is clearly observable in the human knee model presented here (Fig. 3), but was not replicated in the bioreactors simulated. Notably, some bioreactor designs have incorporated sliding motion to capture this phenomenon (Shekhawat et al., 2021; Yuh et al., 2025), representing an important design feature that future *in silico* models should account for.

This study also elucidated the importance of the calcified cartilage layer in reducing stress transfer to the underlying subchondral bone during compression and in acting as an intermediate layer that limits interfacial stresses within cartilage. In this work, calcified cartilage was modeled as a linear elastic material, as its permeability remains poorly defined experimentally. While some studies characterize it as nearly impermeable, others report permeability values lower or comparable to those of articular cartilage (Jönsson et al., 2024). In future studies, experimentally determined permeability should be incorporated into poroelastic FE analyses of OC plugs to capture fluid-mediated (and thereby molecular) cross-talk between cartilage and bone through the calcified cartilage, a process expected to influence and potentially alter the progression of cartilage degeneration in osteoarthritis (Lories and Luyten, 2011).

FE analysis of agarose TE constructs in different bioreactors showed lower maximum principal stresses due to the hydrogel's compliant behavior compared to articular cartilage. Furthermore, the TE constructs were homogeneous and isotropic, producing a more uniform stress distribution than cartilage, where collagen fibril anisotropy generates higher stresses in the SZ. FE analysis also revealed that TE constructs developed lower pore pressures and higher pore fluid velocities for the same magnitudes of mechanical loading as compared to cartilage. The lower pore pressure meant lower load bearing capacity of the construct,

which would restrict its application when implanted *in vivo* in a cartilage defect. Elevated fluid velocities have dual biological consequences: they may enhance nutrient transport and support cartilage regeneration (Sengers et al., 2004), but can also disrupt nascent extracellular matrix secreted by embedded cells, potentially causing matrix loss and weakening the construct (Orozco et al., 2021). To increase the load bearing capacity of such TE constructs, recent studies have introduced micro-fiber reinforcements using the melt electrowriting process. Such reinforced hydrogels are reported to have better mechanical strength and enhanced pore fluid pressurization (Castilho et al., 2018; Moo et al., 2023).

Direct one-to-one comparison between experimentally measured and numerically predicted stress distributions was not feasible due to the difficulty of measuring spatial stress fields in cartilage or TE constructs. The credibility of the FE predictions was therefore assessed qualitatively by comparing predicted stress magnitudes with reported experimental data from similar bioreactor setups. Park et al. (2004) reported Cauchy stresses of 4.79 MPa under 12.7% dynamic compression of bovine cartilage explants, while Rich et al. (2024) measured approximately 1.5 MPa at 20% strain in 3 mm thick human ankle cartilage without preload. In the present FE model, maximum principal stresses at the construct center ranged from 0.67 to 1.83 MPa at 10% compression and 4.89 to 12 MPa at 20% compression (Fig. 5). For agarose TE constructs, Mauck et al. (2000) measured compressive stresses of about 4 kPa and 8 kPa at 10% and 20% strain, whereas our FE models predicted 1.43 kPa and 4.39 kPa, respectively. While the comparative analysis between experiments and FE simulations supported the qualitative credibility of the FE models, several possible factors might influence the credibility assessment. For example, species-specific variations in cartilage properties have been reported in the literature, with bovine cartilage being generally stiffer than human cartilage (Temple et al., 2016), potentially leading to higher measured stresses under comparable strains. Cartilage mechanical properties also vary significantly with anatomical location (Li et al., 2021; Linus et al., 2024). Furthermore, variations in preload, strain rate, and loading frequency affect the magnitude of measured stresses (Patel et al., 2019; Li et al., 2021). Despite these sources of variability, the predicted stress magnitudes were of comparable order to experimentally reported values, supporting the qualitative credibility of the present FE models.

During the unconfined compression of TE constructs, free lateral expansion of the construct was possible, thereby altering the deformation field as compared to native cartilage. To prevent this from happening, and also to reduce fluid flow from the lateral sides of the construct, confinement of the bottom half of the cartilage or TE construct had been suggested by Thorpe et al. (2013). Furthermore, restrictions imposed by the partial confinement on fluid flow and lateral deformations would result in higher pore fluid pressures and also would create a gradient of the mechanical environment that would more closely mimic the *in vivo* mechanics of cartilage.

Beyond the applied mechanical loading regimen, the intrinsic material properties of the TE construct can substantially influence its mechanical behavior. Agarose was selected in this study due to its simplicity and widespread usage in cartilage TE. However, more advanced hydrogels with tunable mechanical properties have been reported in literature that could be incorporated into the *in silico* modeling framework in future work (Ansari et al., 2024; Mukherjee et al., 2025). Moreover, prior experimental studies (Mauck et al., 2000) have shown that the mechanical properties of constructs evolve as cells deposit cartilaginous matrix. Evaluating the FE models across multiple maturation states would therefore offer valuable insight into how developing extracellular matrix alters TE construct mechanics. Incorporation of growth and remodeling formulations (Ateshian et al., 2014; Myers and Ateshian, 2014) represents an important future extension to the FE models developed in this study, that would enable quantification of evolving mechanical behavior in dynamically maturing TE cartilage.

Finally, in the current study, mechanics of articular cartilage and TE constructs were studied at the macro-scale, tissue-level resolution. This approach provided valuable insights into the distribution of physical variables across different setups and under varying loading conditions. However, the present study did not consider cell–matrix interactions, which are known to influence cellular responses to mechanical stimuli (Gao et al., 2014). A more comprehensive and consistent comparison across bioreactor systems could be achieved using multiscale modeling frameworks. In particular, approaches such as that developed by Mukherjee et al. (2026), which employ a post-processing strategy to link tissue-level mechanical fields to cell-scale mechanics and intracellular mechanotransduction pathways, provide a promising direction. In this framework, macroscale displacement and pore pressures are used to define boundary conditions on representative cellular domains using a submodeling technique, enabling the propagation of mechanical stimuli from the tissue to the cellular scale submodel. To connect the cellular scale forces with intracellular gene/protein regulatory network modeling mechanotransduction pathways, Hill-type functions are used. This post-processing approach further enables simulation of multiple cells at varying spatial location of the cartilage simultaneously, thereby addressing the spatial heterogeneity in mechanical stimuli experienced by the cells. By capturing the interactions between tissue mechanics, cellular responses, and intracellular signaling, such multiscale approaches would enable more rigorous comparison and optimization of bioreactor conditions, ultimately facilitating improved and more predictive tissue regeneration strategies.

To conclude, this study establishes an *in silico* framework to benchmark bioreactor loading conditions against *in vivo* joint mechanics. While limited to a single-subject dataset, this methodology provides the tissue engineering community with a comparative template to evaluate current protocols and design more physiologically relevant mechanical stimulation strategies.

CRediT authorship contribution statement

Satanik Mukherjee: Writing – original draft, Methodology, Investigation, Formal analysis, Conceptualization. **Wouter Wilson:** Writing – review & editing, Methodology, Conceptualization. **Liesbet Geris:** Writing – review & editing, Supervision, Funding acquisition, Conceptualization.

Declaration of competing interest

The authors declare the following financial interests/personal relationships which may be considered as potential competing interests: Wouter Wilson reports a relationship with Sioux technologies that includes: employment. If there are other authors, they declare that they have no known competing financial interests or personal relationships that could have appeared to influence the work reported in this paper.

Acknowledgments

This study received funding from the European Union's Horizon 2020 research and innovation programme under the Marie Skłodowska-Curie grant agreement No. 721432 (CarBon project), the In Silico World project (grant agreement No. 101016503), the European Research Council Consolidator Grant No. 101088919 and the Belgian Federal Public Service Policy & Support (grant DigiTwin4PH). The funding sources have no role in design and execution of the study.

Appendix A. Supplementary data

Supplementary material related to this article can be found online at https://doi.org/10.1016/j.jmbbm.2026.107476.

Data availability

Data will be made available on request.

References

Ansari, M., Darvishi, A., Sabzevari, A., 2024. A review of advanced hydrogels for cartilage tissue engineering. Front. Bioeng. Biotechnol. 12, http://dx.doi.org/10.3389/fbioe.2024.1340893, publisher: Frontiers. https://www.frontiersin.org/journals/bioengineering-and-biotechnology/articles/10.3389/fbioe.2024.1340893/full.

Ateshian, G.A., Nims, R.J., Maas, S., Weiss, J.A., 2014. Computational modeling of chemical reactions and interstitial growth and remodeling involving charged solutes and solid-bound molecules. Biomech. Model. Mechanobiol. 13 (5), 1105–1120. http://dx.doi.org/10.1007/s10237-014-0560-1.

Babalola, O.M., Bonassar, L.J., 2009. Element analysis of physical stimuli resulting from mechanical stimulation of tissue engineered cartilage. J. Biomech. Eng. 131 (061014), http://dx.doi.org/10.1115/1.3128672.

Bader, D.L., Salter, D.M., Chowdhury, T.T., 2011. Biomechanical influence of cartilage homeostasis in health and disease. Arthritis 2011, 979032. http://dx.doi.org/10.1155/2011/979032, https://www.ncbi.nlm.nih.gov/pmc/articles/PMC3196252/.

Bandeiras, C., Completo, A., Ramos, A., 2014. Compression, shear and bending on tissue-engineered cartilage: a numerical study. Comput. Methods Biomech. Biomed. Eng. 17 (suppl. 1), 2–3. http://dx.doi.org/10.1080/10255842.2014.931047, https://www.tandfonline.com/doi/abs/10.1080/10255842.2014.931047.

Bonnevie, E.D., Delco, M.L., Bartell, L.R., Jasty, N., Cohen, I., Fortier, L.A., Bonassar, L.J., 2018. Microscale frictional strains determine chondrocyte fate in loaded cartilage. J. Biomech. 74, 72–78. http://dx.doi.org/10.1016/j.jbiomech.2018.04.020, https://www.sciencedirect.com/science/article/pii/S0021929018302938.

Buschmann, M.D., Gluzband, Y.A., Grodzinsky, A.J., Kimura, J.H., Hunziker, E.B., 1992. Chondrocytes in agarose culture synthesize a mechanically functional extracellular matrix. J. Orthop. Res. 10 (6), 745–758. http://dx.doi.org/10.1002/jor.1100100602, https://onlinelibrary.wiley.com/doi/abs/10.1002/jor.1100100602.

Caligaris, M., Ateshian, G.A., 2008. Effects of sustained interstitial fluid pressurization under migrating contact area, and boundary lubrication by synovial fluid, on cartilage friction. Osteoarthr. Cartilage/OARS, Osteoarthr. Res. Soc. 16 (10), 1220–1227. http://dx.doi.org/10.1016/j.joca.2008.02.020, https://pmc.ncbi.nlm.nih.gov/articles/PMC2622427/.

Castilho, M., Hochleitner, G., Wilson, W., van Rietbergen, B., Dalton, P.D., Groll, J., Malda, J., Ito, K., 2018. Mechanical behavior of a soft hydrogel reinforced with three-dimensional printed microfibre scaffolds. Sci. Rep. 8 (1), 1245. http://dx.doi.org/10.1038/s41598-018-19502-y, publisher: Nature Publishing Group. https://www.nature.com/articles/s41598-018-19502-y.

Chariyev-Prinz, F., Szojka, A., Neto, N., Burdis, R., Monaghan, M.G., Kelly, D.J., 2023. An assessment of the response of human MSCs to hydrostatic pressure in environments supportive of differential chondrogenesis. J. Biomech. 154, 111590. http://dx.doi.org/10.1016/j.jbiomech.2023.111590, https://linkinghub.elsevier.com/retrieve/pii/S0021929023001598.

Durney, K.M., Shaeffer, C.A., Zimmerman, B.K., Nims, R.J., Oungoulian, S., Jones, B.K., Boorman-Padgett, J.F., Suh, J.T., Shah, R.P., Hung, C.T., Ateshian, G.A., 2020. Immature bovine cartilage wear by fatigue failure and delamination. J. Biomech. 107, 109852. http://dx.doi.org/10.1016/j.jbiomech.2020.109852, https://www.sciencedirect.com/science/article/pii/S002192902030275X.

Elahi, S.A., Castro-Viñuelas, R., Tanska, P., Korhonen, R.K., Lories, R., Famaey, N., Jonkers, I., 2023. Contribution of collagen degradation and proteoglycan depletion to cartilage degeneration in primary and secondary osteoarthritis: an in silico study. Osteoarthr. Cartil. 31 (6), 741–752. http://dx.doi.org/10.1016/j.joca.2023.01.004, publisher: Elsevier. https://www.oarsijournal.com/article/S1063-4584(23)00022-5/fulltext.

Elahi, S.A., Tanska, P., Mukherjee, S., Korhonen, R.K., Geris, L., Jonkers, I., Famaey, N., 2021. Guide to mechanical characterization of articular cartilage and hydrogel constructs based on a systematic *in silico parameter sensitivity analysis*. J. Mech. Behav. Biomed. Mater. 124, 104795. http://dx.doi.org/10.1016/j.jmbbm.2021.104795, https://www.sciencedirect.com/science/article/pii/S1751616121004367.

Elder, B.D., Athanasiou, K.A., 2009. Hydrostatic pressure in articular cartilage tissue engineering: From chondrocytes to tissue regeneration. Tissue Eng. Part B: Rev. 15 (1), 43–53. http://dx.doi.org/10.1089/ten.teb.2008.0435, https://www.liebertpub.com/doi/10.1089/ten.teb.2008.0435.

Erdemir, A., 2016. Open knee: Open source modeling & simulation to enable scientific discovery and clinical care in knee biomechanics. J. Knee Surg. 29 (2), 107–116. http://dx.doi.org/10.1055/s-0035-1564600, https://www.ncbi.nlm.nih.gov/pmc/articles/PMC4876308/.

Eskelinen, A.S.A., Mononen, M.E., Venäläinen, M.S., Korhonen, R.K., Tanska, P., 2019. Maximum shear strain-based algorithm can predict proteoglycan loss in damaged articular cartilage. Biomech. Model. Mechanobiol. 18 (3), 753–778. http://dx.doi.org/10.1007/s10237-018-01113-1.

Evans, L.A.E., Pitsillides, A.A., 2022. Structural clues to articular calcified cartilage function: A descriptive review of this crucial interface tissue. J. Anat. 241 (4), 875–895. http://dx.doi.org/10.1111/joa.13728, https://onlinelibrary.wiley.com/doi/abs/10.1111/joa.13728.

Gao, Y., Liu, S., Huang, J., Guo, W., Chen, J., Zhang, L., Zhao, B., Peng, J., Wang, A., Wang, Y., Xu, W., Lu, S., Yuan, M., Guo, Q., 2014. The ECM -cell interaction of cartilage extracellular matrix on chondrocytes. Biomed. Res. Int. 2014, 648459. http://dx.doi.org/10.1155/2014/648459, https://www.ncbi.nlm.nih.gov/pmc/articles/PMC4052144/.

Geris, L., Lambrechts, T., Carlier, A., Papantoniou, I., 2018. The future is digital: *in silico tissue engineering*. Curr. Opin. Biomed. Eng. 6, 92–98. http://dx.doi.org/10.1016/j.cobme.2018.04.001, https://www.sciencedirect.com/science/article/pii/{S2468451118300102}.

Geurds, L., Xu, Y., Stokes, J.R., 2021. Friction of lubricated hydrogels: Influence of load, speed and lubricant viscosity. Biotribology 25, 100162. http://dx.doi.org/10.1016/j.biotri.2021.100162, https://www.sciencedirect.com/science/article/pii/S2352573821000032.

Gilbert, S.J., Blain, E.J., 2018. Chapter 4 - cartilage mechanobiology: How chondrocytes respond to mechanical load. In: Verbruggen, S.W. (Ed.), Mechanobiology in Health and Disease. Academic Press, pp. 99–126. http://dx.doi.org/10.1016/B978-0-12-812952-4.00004-0, https://www.sciencedirect.com/science/article/pii/B9780128129524000040.

Grad, S., Loparic, M., Peter, R., Stolz, M., Aebi, U., Alini, M., 2012. Sliding motion modulates stiffness and friction coefficient at the surface of tissue engineered cartilage. Osteoarthr. Cartil. 20 (4), 288–295. http://dx.doi.org/10.1016/j.joca.2011.12.010, https://www.sciencedirect.com/science/article/pii/S1063458412000143.

Griffin, T.M., Guilak, F., 2005. The role of mechanical loading in the onset and progression of osteoarthritis. Exerc. Sport. Sci. Rev. 33 (4), 195–200. http://dx.doi.org/10.1097/00003677-200510000-00008.

Guilak, F., 2005. The slippery slope of arthritis. Arthritis Rheum. 52 (6), 1632–1633. http://dx.doi.org/10.1002/art.21051, https://onlinelibrary.wiley.com/doi/10.1002/art.21051.

Hassan, C.R., Qin, Y.-X., Komatsu, D.E., Uddin, S.M., 2019. Utilization of finite element analysis for articular cartilage tissue engineering. Mater. (Basel) 12 (20), 3331. http://dx.doi.org/10.3390/ma12203331, https://www.ncbi.nlm.nih.gov/pmc/articles/PMC6829543/.

Hodder, E., Guppy, F., Covill, D., Bush, P., 2020. The effect of hydrostatic pressure on proteoglycan production in articular cartilage in vitro: a meta-analysis. Osteoarthr. Cartil. 28 (8), 1007–1019. http://dx.doi.org/10.1016/j.joca.2020.03.021, https://linkinghub.elsevier.com/retrieve/pii/S1063458420310256.

Jönsson, V., Orozco, G.A., Pierantoni, M., Dejea, H., Gustafsson, A., Grassi, L., Isaksson, H., 2024. Influence of articular cartilage sample geometry on mechanical response and properties using finite element simulation. J. Biomech. 176, 112323. http://dx.doi.org/10.1016/j.jbiomech.2024.112323, https://www.sciencedirect.com/science/article/pii/S0021929024004019.

Khoshgoftar, M., van Donkelaar, C.C., Ito, K., 2011. Mechanical stimulation to stimulate formation of a physiological collagen architecture in tissue-engineered cartilage: a numerical study. Comput. Methods Biomech. Biomed. Eng. 14 (2), 135–144. http://dx.doi.org/10.1080/10255842.2010.519335.

Kleuskens, M.W.A., van Donkelaar, C.C., Kock, L.M., Janssen, R.P.A., Ito, K., 2021. An ex vivo human osteochondral culture model. J. Orthop. Res. 39 (4), 871–879. http://dx.doi.org/10.1002/jor.24789, https://onlinelibrary.wiley.com/doi/abs/10.1002/jor.24789.

Kosonen, J.P., Eskelinen, A.S.A., Orozco, G.A., Nieminen, P., Anderson, D.D., Grodzinsky, A.J., Korhonen, R.K., Tanska, P., 2023. Injury-related cell death and proteoglycan loss in articular cartilage: Numerical model combining necrosis, reactive oxygen species, and inflammatory cytokines. PLoS Comput. Biol. 19 (1), e1010337. http://dx.doi.org/10.1371/journal.pcbi.1010337, https://pmc.ncbi.nlm.nih.gov/articles/PMC9879441/.

Li, Y., Frank, E.H., Wang, Y., Chubinskaya, S., Huang, H.-H., Grodzinsky, A.J., 2013. Moderate dynamic compression inhibits pro-catabolic response of cartilage to mechanical injury, tumor necrosis factor-a and interleukin-6, but accentuates degradation above a strain threshold. Osteoarthr. Cartil. 21 (12), 1933–1941. http://dx.doi.org/10.1016/j.joca.2013.08.021, https://www.oarsijournal.com/article/S1063-4584(13)00939-4/fulltext.

Li, H., Li, J., Yu, S., Wu, C., Zhang, W., 2021. The mechanical properties of tibiofemoral and patellofemoral articular cartilage in compression depend on anatomical regions. Sci. Rep. 11, 6128. http://dx.doi.org/10.1038/s41598-021-85716-2, https://pmc.ncbi.nlm.nih.gov/articles/PMC7969630/.

Linus, A., Tanska, P., Nippolainen, E., Tiitu, V., Töyras, J., Korhonen, R.K., Afara, I.O., Mononen, M.E., 2024. Site-specific elastic and viscoelastic biomechanical properties of healthy and osteoarthritic human knee joint articular cartilage. J. Biomech. 169, 112135. http://dx.doi.org/10.1016/j.jbiomech.2024.112135, https://www.sciencedirect.com/science/article/pii/S0021929024002136.

Lories, R.J., Luyten, F.P., 2011. The bone–cartilage unit in osteoarthritis. Nat. Rev. Rheumatol. 7 (1), 43–49. http://dx.doi.org/10.1038/nrrheum.2010.197, https://www.nature.com/articles/nrrheum.2010.197.

Mauck, R.L., Soltz, M.A., Wang, C.C.B., Wong, D.D., Chao, P.-H.G., Valhmu, W.B., Hung, C.T., Ateshian, G.A., 2000. Engineering of articular cartilage through dynamic loading of chondrocyte-seeded agarose gels. J. Biomech. Eng. 122 (3), 252–260. http://dx.doi.org/10.1115/1.429656.

Mononen, M.E., Jurvelin, J.S., Korhonen, R.K., 2015. Implementation of a gait cycle loading into healthy and meniscectomised knee joint models with fibril-reinforced articular cartilage. Comput. Methods Biomech. Biomed. Eng. 18 (2), 141–152.

http://dx.doi.org/10.1080/10255842.2013.783575, https://www.tandfonline.com/doi/abs/10.1080/10255842.2013.783575.

Mononen, M.E., Tanska, P., Isaksson, H., Korhonen, R.K., 2016. A novel method to simulate the progression of collagen degeneration of cartilage in the knee: data from the osteoarthritis initiative. Sci. Rep. 6 (1), 21415. http://dx.doi.org/10.1038/srep21415, publisher: Nature Publishing Group. https://www.nature.com/articles/srep21415.

Moo, E.K., Ebrahimi, M., Hrynevich, A., de Ruijter, M., Castilho, M., Malda, J., Korhonen, R.K., 2023. Load-induced fluid pressurisation in hydrogel systems before and after reinforcement by melt-electrowritten fibrous meshes. J. Mech. Behav. Biomed. Mater. 143, 105941. http://dx.doi.org/10.1016/j.jmbbm.2023.105941, https://www.sciencedirect.com/science/article/pii/S1751616123002941.

Mukherjee, S., Lesage, R., Geris, L., 2026. A multiscale modeling approach to study the role of mechanics and inflammation in the pathophysiology of articular cartilage. Comput. Biol. Med. 211, 111737. http://dx.doi.org/10.1016/j.compbiomed.2026.111737, https://www.sciencedirect.com/science/article/pii/S001048252600301X.

Mukherjee, S., Nazemi, M., Jonkers, I., Geris, L., 2020. Use of computational modeling to study joint degeneration: A review. Front. Bioeng. Biotechnol. 8, http://dx.doi.org/10.3389/fbioe.2020.00093, https://www.frontiersin.org/journals/bioengineering-and-biotechnology/articles/10.3389/fbioe.2020.00093/full.

Mukherjee, S., Senol, S., Hegde, S., Chandrakar, A., Moroni, L., Wieringa, P., Geris, L., 2025. Experimentally-informed *in silico design of melt-electrowritten scaffolds for tissue engineering applications*. Mater. Des. 258, 114603. http://dx.doi.org/10.1016/j.matdes.2025.114603, https://www.sciencedirect.com/science/article/pii/S0264127525010238.

Myers, K., Ateshian, G.A., 2014. Interstitial growth and remodeling of biological tissues: Tissue composition as state variables. J. Mech. Behav. Biomed. Mater. 29, 544–556. http://dx.doi.org/10.1016/j.jmbbm.2013.03.003, https://www.sciencedirect.com/science/article/pii/S1751616113000817.

Natenstedt, J., Kok, A.C., Dankelman, J., Tuijthof, G.J., 2015. What quantitative mechanical loading stimulates in vitro cultivation best? J. Exp. Orthop. 2 (1), 15. http://dx.doi.org/10.1186/s40634-015-0029-x.

Neu, C.P., Hull, M.L., Walton, J.H., 2005. Heterogeneous three-dimensional strain fields during unconfined cyclic compression in bovine articular cartilage explants. J. Orthop. Res. 23 (6), 1390–1398. http://dx.doi.org/10.1016/j.orthres.2005.03.022.1100230622.

Ogawa, H., Kozhemyakina, E., Hung, H.-H., Grodzinsky, A.J., Lassar, A.B., 2014. Mechanical motion promotes expression of Prg4 in articular cartilage via multiple CREB-dependent, fluid flow shear stress-induced signaling pathways. Genes Dev. 28 (2), 127–139. http://dx.doi.org/10.1101/gad.231969.113, https://pmc.ncbi.nlm.nih.gov/articles/PMC3909787/.

Orozco, G.A., Bolcos, P., Mohammadi, A., Tanaka, M.S., Yang, M., Link, T.M., Ma, B., Li, X., Tanska, P., Korhonen, R.K., 2021. Prediction of local fixed charge density loss in cartilage following ACL injury and reconstruction: A computational proof-of-concept study with MRI follow-up. J. Orthop. Res. 39 (5), 1064–1081. http://dx.doi.org/10.1002/jor.24797, https://onlinelibrary.wiley.com/doi/abs/10.1002/jor.24797.

Orozco, G.A., Tanska, P., Florea, C., Grodzinsky, A.J., Korhonen, R.K., 2018. A novel mechanobiological model can predict how physiologically relevant dynamic loading causes proteoglycan loss in mechanically injured articular cartilage. Sci. Rep. 8 (1), 15599. http://dx.doi.org/10.1038/s41598-018-33759-3, publisher: Nature Publishing Group. https://www.nature.com/articles/s41598-018-33759-3.

Park, S., Hung, C.T., Ateshian, G.A., 2004. Mechanical response of bovine articular cartilage under dynamic unconfined compression loading at physiological stress levels. Osteoarthr. Cartil. 12 (1), 65–73. http://dx.doi.org/10.1016/j.joca.2003.08.005, publisher: Elsevier. https://www.oarsijournal.com/article/S1063-4584(03)00217-6/fulltext#FIG2.

Patel, J.M., Wise, B.C., Bonnevie, E.D., Mauck, R.L., 2019. A systematic review and guide to mechanical testing for articular cartilage tissue engineering. Tissue Eng. Part C: Methods 25 (10), 593–608. http://dx.doi.org/10.1089/ten.tec.2019.0116, https://www.liebertpub.com/doi/10.1089/ten.tec.2019.0116.

Petersen, C.A., Sise, C.V., Dewing, J.X., Yun, J., Zimmerman, B.K., Guo, X.E., Hung, C.T., Ateshian, G.A., 2023. Immature bovine cartilage wear is due to fatigue failure from repetitive compressive forces and not reciprocating frictional forces. Osteoarthr. Cartil. 31 (12), 1594–1601. http://dx.doi.org/10.1016/j.joca.2023.08.008, https://www.sciencedirect.com/science/article/pii/S1063458423008920.

Quiroga, J.M.P., Wilson, W., Ito, K., van Donkelaar, C.C., 2017. Relative contribution of articular cartilage's constitutive components to load support depending on strain rate. Biomech. Model. Mechanobiol. 16 (1), 151–158. http://dx.doi.org/10.1007/s10237-016-0807-0.

Rapagna, S., Roberts, B.C., Solomon, L.B., Reynolds, K.J., Thewlis, D., Perilli, E., 2021. Tibial cartilage, subchondral bone plate and trabecular bone microarchitecture in varus- and valgus-osteoarthritis versus controls. J. Orthop. Res. 39 (9), 1988–1999. http://dx.doi.org/10.1002/jor.24914, https://onlinelibrary.wiley.com/doi/abs/10.1002/jor.24914.

Rich, M.J., Burnash, S., Krishnan, R.R., Chubinskaya, S., Loeser, R.F., Polacheck, W.J., Diekman, B.O., 2024. Use of a novel magnetically actuated compression system to study the temporal dynamics of axial and lateral strain in human osteochondral plugs. J. Biomech. 162, 111887. http://dx.doi.org/10.1016/j.jbiomech.2023.111887, https://www.sciencedirect.com/science/article/pii/S002192902300458X.

Sah, R.L.-Y., Kim, Y.-J., Doong, J.-Y.H., Grodzinsky, A.J., Plass, A.H.K., Sandy, J.D., 1989. Biosynthetic response of cartilage explants to dynamic compression. J. Orthop. Res. 7 (5), 619–636. http://dx.doi.org/10.1002/jor.1100070502, https://onlinelibrary.wiley.com/doi/abs/10.1002/jor.1100070502.

Salinas, E.Y., Hu, J.C., Athanasiou, K., 2018. A guide for using mechanical stimulation to enhance tissue-engineered articular cartilage properties. Tissue Eng. Part B: Rev. 24 (5), 345–358. http://dx.doi.org/10.1089/ten.teb.2018.0006, https://www.liebertpub.com/doi/10.1089/ten.teb.2018.0006.

Schwab, A., Buss, A., Pullig, O., Ehlicke, F., 2021. Ex vivo osteochondral test system with control over cartilage defect depth – A pilot study to investigate the effect of oxygen tension and chondrocyte based treatments in chondral and full thickness defects in an organ model. Osteoarthr. Cartil. Open 3 (2), 100173. http://dx.doi.org/10.1016/j.ocarto.2021.100173, https://www.sciencedirect.com/science/article/pii/S2665913121000364.

Sengers, B.G., Oomens, C.W.J., Baaijens, F.P.T., 2004. An integrated finite-element approach to mechanics, transport and biosynthesis in tissue engineering. J. Biomech. Eng. 126 (1), 82–91. http://dx.doi.org/10.1115/1.1645526, https://asmedigitalcollection.asme.org/biomechanical/article/126/1/82/464861/An-Integrated-FiniteElement-Approach-to-Mechanics.

Shekhawat, V.K., Hamilton, J.L., Pacione, C.A., Schmid, T.M., Wimmer, M.A., 2021. A moving contact of articulation enhances the biosynthetic and functional responses of articular cartilage. Biotribology (Oxford) 26, 100180. http://dx.doi.org/10.1016/j.biotri.2021.100180, https://pmc.ncbi.nlm.nih.gov/articles/PMC8064563/.

Stender, M.E., Regueiro, R.A., Ferguson, V.L., 2017. A poroelastic finite element model of the bone–cartilage unit to determine the effects of changes in permeability with osteoarthritis. Comput. Methods Biomech. Biomed. Eng. 20 (3), 319–331. http://dx.doi.org/10.1080/10255842.2016.1233326, https://www.tandfonline.com/doi/full/10.1080/10255842.2016.1233326.

Tanck, E., van Driel, W.D., Hagen, J.W., Burger, E.H., Blankevoort, L., Huiskes, R., 1999. Why does intermittent hydrostatic pressure enhance the mineralization process in fetal cartilage? J. Biomech. 32 (2), 153–161. http://dx.doi.org/10.1016/S0021-9290(98)00165-1, https://www.sciencedirect.com/science/article/pii/S0021929098001651.

Temple, D.K., Cederlund, A.A., Lawless, B.M., Aspden, R.M., Espino, D.M., 2016. Viscoelastic properties of human and bovine articular cartilage: a comparison of frequency-dependent trends. BMC Musculoskelet. Disord. 17 (1), 419. http://dx.doi.org/10.1186/s12891-016-1279-1.

Thorpe, S.D., Nagel, T., Carroll, S.F., Kelly, D.J., 2013. Modulating gradients in regulatory signals within mesenchymal stem cell seeded hydrogels: A novel strategy to engineer zonal articular cartilage. PLoS One 8 (4), e60764. http://dx.doi.org/10.1371/journal.pone.0060764, https://journals.plos.org/plosone/article?id=10.1371/journal.pone.0060764.

Vainieri, M.L., Wahl, D., Alini, M., van Osch, G.J.V.M., Grad, S., 2018. Mechanically stimulated osteochondral organ culture for evaluation of biomaterials in cartilage repair studies. Acta Biomater. 81, 256–266. http://dx.doi.org/10.1016/j.actbio.2018.09.058, https://www.sciencedirect.com/science/article/pii/S1742706118305877.

Wilson, W., van Donkelaar, C.C., van Rietbergen, B., Ito, K., Huiskes, R., 2004. Stresses in the local collagen network of articular cartilage: a poroviscoelastic fibril-reinforced finite element study. J. Biomech. 37 (3), 357–366. http://dx.doi.org/10.1016/S0021-9290(03)00267-7, https://www.sciencedirect.com/science/article/pii/S0021929003002677.

Wimmer, M.A., Grad, S., Kaup, T., Hänni, M., Schneider, E., Gogolewski, S., Alini, M., 2004. Tribology approach to the engineering and study of articular cartilage. Tissue Eng. 10 (9–10), 1436–1445. http://dx.doi.org/10.1089/ten.2004.10.1436, publisher: SAGE Publications. https://journals.sagepub.com/action/showAbstract.

Yuh, C., Laurent, M.P., Torzilli, P.A., Mell, S.P., Maher, S.A., Chubinskaya, S., Wimmer, M.A., 2025. Effects of kinematic and kinetic variables on articular cartilage mechanical and biological properties. Osteoarthr. Cartil. 33 (6), 710–720. http://dx.doi.org/10.1016/j.joca.2025.02.790, https://www.sciencedirect.com/science/article/pii/S1063458425008635.

Zahedmanesh, H., Stoddart, M., Lezuo, P., Forkmann, C., Wimmer, M.A., Alini, M., Oosterwyck, H. Van, 2014. Deciphering mechanical regulation of chondrogenesis in fibrin–polyurethane composite scaffolds enriched with human mesenchymal stem cells: a dual computational and experimental approach. Tissue Engi. Part A 20 (19-20), 2615–2626. http://dx.doi.org/10.1089/ten.tea.2013.0145.